J Mater Sci (2007) 42:8203–8208
DOI 10.1007/s10853-007-1735-2

Stress characterization of surface damages on soda-lime glass using a nanocontact deformation method

Yun-Hee Lee · Ju-Young Kim · Unbong Baek · Seung-Hoon Nahm

Received: 20 August 2006 / Accepted: 29 March 2007 / Published online: 9 June 2007

Abstract A nanocontact deformation method was used to measure the local and graded residual stresses around contact damages. By analyzing influences of the residual stress on nanocontact deformation itself instead of measuring the secondary crack emanated from it, 0.65 μm spatial resolution, which was superior to the highest level 1.8 μm attained by previous indentation fracture mechanics tests with an acute cube-corner indenter, was obtained with a general Berkovich indenter. However, a stress model combined with the nanocontact deformation provided only average stress variation around the contact damages. Thus, a resolution of two principal components from the residual stress in a biaxial state has been attempted in this study. By introducing radial microcracks around artificial microVickers damages, a crack-normal circumferential stress component disappeared and a series of nanoindentations close to the microcrack line yielded a variation of the radial stress component. By comparing this result with the average stress variation mentioned above, the crack-opening circumferential stress was measured and showed a good consistency with the previous study in soda-lime glass. In addition, distinctive features of present method were compared with previous indentation fracture mechanics method.

Y.-H. Lee (✉) · U. Baek · S.-H. Nahm
Division of Metrology for Quality Life, Korea Research Institute of Standards and Science, Daejeon 305-340, Korea
e-mail: uni44@kriss.re.kr

J.-Y. Kim
School of Materials Science and Engineering, Seoul National Univeristy, Seoul 151-742, Korea

Introduction

Brittle solids implying surface contact damages generally have lower strength, wear resistance [1, 2], and fatigue properties due to the damage-induced residual stresses and their roles in accelerating microcracks [3]. Although an experimental measurement of the residual stresses around local contact damages comes into an important issue, this is still difficult due to their complex and rapid distribution over the local damage site. Optical photoelasticity [4] interpreting stress-induced fringe is applicable to few transparent materials. Raman luminescence microscopy [5, 6] needs an empirical conversion factor for quantifying a stress value from the peak shift.

A stress measurement based on the indentation fracture mechanics method was firstly proposed by Zeng and Rowcliffe [7]: here the residual stress is measured from dimension of the spontaneous microcrack emanated from a microindent. A microindentation having the capacity of making the microcrack length c_0 in stress-free state can induce the microcrack dimension c_R in stressed state because the original crack driving force can be increased (or decreased) by the crack opening behavior of tensile residual stress (or by the crack closing behavior of compressive residual stress). When a composite stress intensity factor formed by the indentation and residual stress is equated to the sample fracture toughness, the stress-influenced microcrack c_R yields a quantitative residual stress σ_{res}. Since a relative distance between the location of the indentation and the end of the microcrack where the stress intensity is measured reduces a spatial resolution of the indentation fracture mechanics method and limits its applications to severely stress-graded samples, a reduction of the crack dimension by adopting a sharper indenter becomes a good research issue [8, 9]. Kese and Rowcliffe

[8] reduced the microcrack size from 60 μm under a microVickers indenter to 1.8 μm by using a cube-corner indenter. A cross-sectional morphology of the microcrack was observed to confirm its stress intensity factor. This indenter tip modification enhances the spatial resolution of the indentation fracture mechanics method but still measures a residual stress value averaged over the microcrack length. In addition, the microcrack must be controlled to be put perpendicular to the residual stress direction to enhance the stress sensitivity. These restrict applications of the indentation fracture method to local regions in a submicron order and severely stress-graded samples. Lately there was an attempt to infer fracture property and critical cracking stress in some glasses from an opening displacement of indentation cracks [10, 11]. But it only provides information upon the crack opening tensile stress and requires a precise measurement of the crack opening displacement with accuracy of more than ±5 nm.

In this study, we have tried to apply the stress-probing nanocontact method [12, 13] bringing about only deformation without any crack development for the characterization of residual stress fields around contact damages. This method examines influences of the residual stress on the indenting deformation and records stress-influenced nanoindentation loading curve. The spatial resolution of this method is much higher than previous indentation fracture mechanics method [7, 8] because the nanoindentation point coincides with the stress-probing location exactly. In detail, the spatial resolution depends on the dimension of the plastic zone and is attainable higher than 100 nm because reproducible nanoindentations shallower than 10 nm depth have been reported under a well-controlled testing condition [14]. Furthermore, it is the first time that the nanocontact deformation has been applied to actual graded stress measurement instead of the previous model-confirmation tests [12, 13] in artificial uniform stresses. Two components in a biaxial stress are resolved by acquiring essential stress ratio from the spontaneous surface cracking event around contact damages. In addition, the peak magnitude of the microcrack-driving stress in soda-lime glass is calculated and compared to previous results.

Theoretical background

Lee et al. [12, 13] have developed a theoretical foundation for measuring a uniform and isotropic stress from the differences in two nanoindentation responses from virgin and stressed surfaces; the indentation load L^0 necessary for attaining a given indenter penetration h_t in virgin surface increases to L^C (or decreases to L^T) in compressively (or tensilely) stressed surface due to the stress-induced change in the penetration resistance of the indented surface. This load shift L^0–L^C is equated with a product of the plastic deformation-activating shear portion in the residual stress $2\sigma^{res}_{avg}/3$ and its supporting contact area A^C_C. Thus the isotropic residual stress σ^{res}_{avg} is defined by $3(L^0 - L^C)/(2A^C_C)$ [13]. When this formulation is applied to a general surface stress having different two principal components, the result corresponds to the mean value of the biaxial stress or $(\sigma^{res}_x + \sigma^{res}_y)/2$. σ^{res}_x and σ^{res}_y are the major and minor principal stress components, respectively, of which σ^{res}_y can be expressed as $\kappa\sigma^{res}_x$ by defining κ as the ratio of two principal stress components. For a given κ value, the residual stress model is extended into the general form in Eq. 1 [13].

$$\sigma^{res}_x = \frac{3(L^0 - L^C)}{(1 + \kappa)A^C_C}. \quad (1)$$

In order to resolve stress component from complex biaxial stress around contact damage using Eq. 1, we propose a stress elimination method for measuring κ value; when a microcrack is introduced into a biaxially stressed region, the stress component perpendicular to the crack plane disappears and thereby making κ into zero in Eq. 1. Thus, by comparing the mean stress and major principal stress component near contact damages respectively before and after microcracking, the other minor stress component can be also calculated.

Experimental procedures

The material studied here is a commercial soda-lime glass (Knittel glaser, Braunschweig, Germany) whose noncrystalline characteristic confirms isotropic elastic/plastic deformation. A microVickers hardness tester (MVK-H2, Akashi Corp., Yokohama Japan) was used to form reproducible contact damages intentionally. By applying the peak indentation load of 0.98 N, some corners among four in microVickers indent were partially cracked and resulted in two stress states of $(\sigma^{res}_{rad}, \sigma^{res}_{cir})$ and $(\sigma^{res}_{rad}, 0)$ corresponding to the uncracked and cracked corners, respectively. Here σ^{res}_{rad} and σ^{res}_{cir} are the radial and circumferential stress components around the microVickers damages, respectively. The major stress component σ^{res}_{rad} between the two corresponds to σ^{res}_x in Eq. 1.

In order to probe these stress regions, Berkovich nanoindentations were performed using a Triboscope module (Hysitron, Inc., MN, USA) coupled to a Nanoscope II atomic force microscope (Veeco Metrology, CA, USA), which provided the images of surface topography before and after each nanoindentation test. The load and displacement resolutions of the nanoindentation module

are 0.1 μN and 0.1 nm, respectively. The indentation load and speed selected for this experiment were 2 mN and 250 μN/s. Each nanoindentation point was controlled to be about 1500 nm from the adjacent nanoindents and microcracks. In addition, several nanoindentation curves were also obtained from an unstressed bare glass to compare with the nanoindentation data close to the microVickers damages.

Results and discussion

Nanoindentation data around remnant microVickers indents

The microVickers indentations produced contact impressions of 9.7 ± 0.2 μm in a half-diagonal dimension, with 7.8 ± 0.3 μm-long radial cracks preceding some corners (see Fig. 1). This partial radial cracking is attributed to inhomogeneous shear fault distribution inside of the microVickers impressions [15, 16]. Uncracked corners were assumed to be in an unstable state susceptible to microcracking and when the specimen was immersed in water for 5 min after all experiments, equivalent radial cracks were observed from all corners of the indents (except for some instances of crack branch or path deviation). This supports that the biaxial stress fields ahead of the four corners in microVickers indent are identical before the formation of the radial crack. The nanoindentations around the microVickers damages retailed remnant test patterns, as shown in Fig. 1. Comparing to the reference nanoindentation curve of the bare glass, two nanoindentation curves from the uncracked and cracked corners of the microVickers damage showed leftward curve shift or compressive stress sign regardless of the presence of the radial crack. In detail, the nanoindentation curve in the cracked corner was located in the left side of that in the uncracked corner, displaying the increase of compressive stress effect by the spontaneous radial cracking (see Fig. 2). This phenomenon is, however, explained by a crack-induced relaxation of the tensile circumferential stress component instead of the actual increase of compressive stress during the radial cracking.

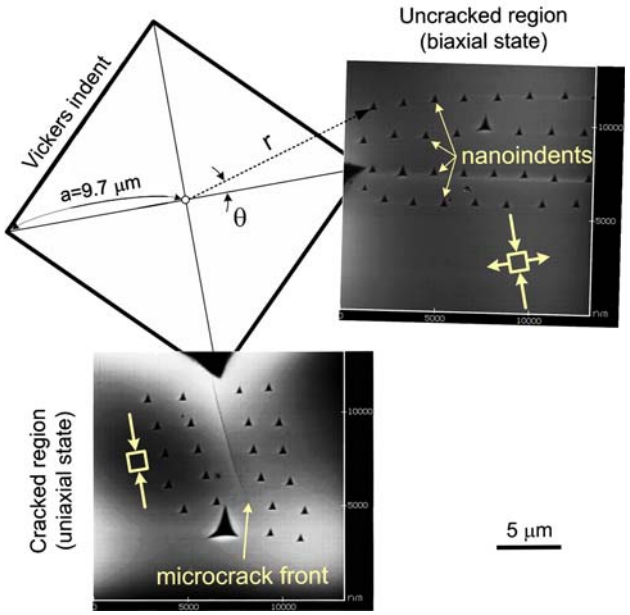

Fig. 1 AFM topographies for nanoindentation arrays formed around a partially cracked microVickers indent

Interpretation of contact residual stresses

In order to interpret quantitative stresses using Eq. 1, amount of the stress-induced curve shift L^0–L^C and the contact area in the stress state A_C^C must be analyzed from the nanoindentation data. L^0–L^C discerned in Fig. 2 is calculated numerically by inserting an analyzing depth into two power-law-fitted loading curves from the unstressed bare glass and the stress-affected zone close to the microVickers damage (see Table 1). A_C^C can be estimated from the unstressed contact area A_C^0 determined from the Oliver-Pharr analysis [17] because the hardness H is independent of the elastic residual stress (i.e. L^0/A_C^0 in the unstressed state has same value of L^C/A_C^C in the tensile stress state) [12, 13]. The contact depth based on the Oliver-Pharr analysis at indentation load 2 mN were 90.95 ± 0.16 nm and resulting hardness was 6.37 ± 0.02 GPa for the virgin soda-lime glass. The contact radius a_C corresponding to 2 mN was 316.24 ± 0.45 nm and the plastic zone radius a_P was predicted by 651.95 ± 0.92 nm by considering the Hill's spherical cavity model in Eq. 2 [18, 19].

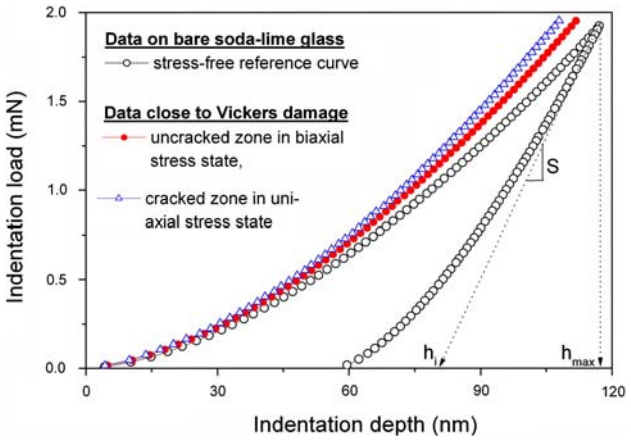

Fig. 2 Comparison of nanoindentation curves from regions near to and far from the microVickers damages

Table 1 Empirical fits of the nanoindentation curves obtained from the microVickers indents and their relative testing locations

Uncracked corner (κ = +1.0)		Cracked corner (κ = 0)	
Distance (μm)	Power-fitted function	Distance (μm)	Power-fitted function
10.56	$L = 0.91\ h^{1.63}$	10.57	$L = 0.94\ h^{1.62}$
12.05	$L = 0.89\ h^{1.63}$	12.20	$L = 0.92\ h^{1.63}$
14.77	$L = 0.87\ h^{1.64}$	14.34	$L = 0.85\ h^{1.64}$
16.37	$L = 0.99\ h^{1.61}$	16.22	$L = 0.87\ h^{1.64}$
18.89	$L = 0.91\ h^{1.63}$	Reference loading curve of bare glass	
20.80	$L = 0.90\ h^{1.63}$	$L = 0.77 \pm 0.02\ h^{1.64 \pm 0.01}$	

$$\frac{a_P}{a_C} = \left(\frac{E}{3(1 - \nu)Y}\right)^{1/3}. \quad (2)$$

Here the Young's modulus E, Poisson's ratio ν and yield strength Y of the soda-lime glass were 69 GPa, 0.25 and 3.5 GPa, respectively. The spatial resolution of this nanocontact deformation method corresponds to the plastic zone dimension and it means the residual stress in this study is an average value over 0.65 μm length.

The trend of radial stress σ_{rad}^{res} in Fig. 3 showed a decaying behavior against distance from the microVickers indent center r. The data points excepting few underestimates were empirically fitted: σ_{rad}^{res} was a function of r to the –0.23 power whose peak value was about –2.15 GPa at the microVickers indent edge. This compressive stress level at the vicinity of the contact damages is conceivable if the yield strength 3.5 GPa of the soda-lime glass is taken into account [18]. Few nanoindentation points about 1500 nm apart from the microcrack line, however, yielded a series of stress underestimates, which could be attributed to an edge effect. Schwarzer et al. [20] reported that the minimum distance to obtain nanoindentation data free from the edge effect or microcrack influence is eight times the contact radius; for the nanoindentation in this study, the minimum distance necessary for avoiding the edge effect is about 2500 nm and thereby making few data close to microcrack meaningless. However, if the residual stress fields have significant variation along the circumferential direction θ shown in Fig. 1, the radial stress profile measured in Fig. 3 can be different from the targeted one along the cracking direction.

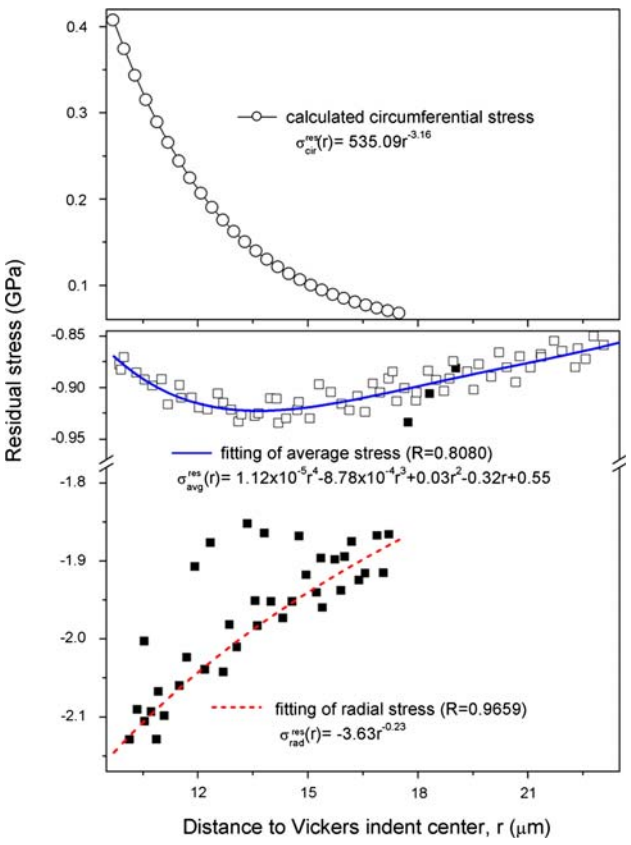

Fig. 3 Local stress distributions around remnant microVickers indents; the radial, circumferential components, and their average stress interpreted from nanoindentation data

The stress measured in the uncracked corner, representing the average response of the circumferential and radial stress components or $(\sigma_{cir}^{res} + \sigma_{rad}^{res})/2$, showed a complex rise and fall behavior; the polynomial fitting function of the average stress in Fig. 3 increased in a negative sense within the near-field region up to r = 13.6 μm and decayed slowly beyond this point (in the far-field region). In addition, the stress data obtained from beyond the microcrack front converges to the average stress trend from the uncracked corner due to the negligible crack-induced stress relaxation.

A stress resolution of this nanocontact deformation method was confirmed by determining a detectable limit of the stress-induced load shift, discriminating the stress influence against the background load fluctuation [13]. By regarding the lower bound at maximum depth about ± 5.3 μN, the stress uncertainty calculated was ±25 MPa near the indented site.

Distribution of critical crack-opening stress

The distribution of the crack-opening circumferential stress σ_{cir}^{res} was calculated by subtracting σ_{rad}^{res} from a double of the

Table 2 Distinctive features of present nanocontact deformation method comparing with previous indentation fracture mechanics method [8]

	Proposed nanocontact deformation method	Kese & Rocliffe's indentation fracture mechanics method [8]
Stress-probing parameter	Shape of nanoindentation loading curve (or plastic zone development in a submicron scale)	Indentation-induced crack growth in a micron scale
Spatial resolution	Depending on the dimension of nanocontact plastic zone	Depending on the shortest indentation microcrack
	Plastic zone $\leq$ 100 nm is possible with a commercial nanoindenter *(reliable nanoindentation shallower than 10 nm has been reported [14] and 0.65 μm spatial resolution in this study can be enhanced by lowering the nanoindentation load)*	Limited spatial resolution due to the cracking threshold *(1.8 μm-long crack is the highest level attainable with the acute cube-corner tip)*
	Dense stress probes within a local targeted region; 1.5 μm spaced nanoindents within 20 μm range around a microVickers damage	Sparse stress probes around a wide targeted region; 50 μm spaced indents within 800 μm range around a Vickers damage
Tip orientation & indenting array	No need for considering indenter tip orientation or array pattern of nanoindents	Concentric indents array having a targeted Vickers damage at their center
		Microcrack originated from one corner of the cube-corner indent must propagate vertical to the residual stress direction to be probed
Issues in application	Applicable to various materials including ductile and brittle solids	Applicable to brittle solids only
	The spontaneous radial cracking proposed in present study for measuring the stress ratio κ in Eq. 1 is applicable to only brittle solids	Not applicable to submicron thin film due to low spatial resolution and vague stress intensity factor of an underdeveloped crack
	A separated κ measuring method must be developed for resolve two residual stress components in ductile metals	Difficulty in measuring microcrack size due to the slow crack growth under humid environment
		Difficulty in controlling cracking direction for crystalline solids having cleavage planes

average stress. As might be expected, σ_{cir}^{res} had crack-opening positive sign and fell rapidly with distance from the microVickers indent center r, thereby constraining any large extension of the radial crack. The actual power of the predicted circumferential stress, plotted against r, was –3.16, above that of the radial stress but close to the predicted value –3.0 of the theoretical indentation-stress models developed by Hill [19] and Yoffe [21].

Furthermore, the peak magnitude of the circumferential stress $(\sigma_{cir}^{res})_{max}$ was calculated as 406.7 MPa at the microVickers indentation edge or r = a and this value could be compared with experimental results [8, 10, 11, 20–22] on the indentation cracking threshold. Lawn and Evans [22] have presented the following equation of the critical dimension of median-radial crack c_0^*.

$$c_0^* = 1.767 \frac{K_C^2}{(\xi H)^2}. \quad (3)$$

Here ξ is the dimensionless parameter related to the cracking threshold and ξH is defined by the peak magnitude of the crack-opening stress. According to c_0^* determination methods, $(\sigma_{cir}^{res})_{max}$ had a wide range of 0.02H to 0.2H [23]. By approximating the critical crack dimension c_0^* as the half-diagonal a of the Vickers indent [24], we could calculate the peak stress magnitude 298.8 MPa comparable with the present result. In addition, Kese and Rowcliffe [8] obtained the peak opening stress close to 400 MPa along the direction highly deviated from the radial crack. The residual stress distribution analyzed from the measurement of crack-opening displacements (COD) along the radial crack [10, 11] showed similar decaying behavior with present results but yielded much higher peak stress of 1.24 GPa for soda-lime glass. The discrepancy between peak stress values from current nanoindentation and COD measurement [11] can be ascribed to the limitation of current nanoindentation in measuring the targeted zone close to the radial crack. As mentioned in 'Nanoindentation data around remnant microVickers indents', the radial stress data obtained from more than 2500 nm apart from the crack line where is free from the edge effect [20] can represent stress distribution somewhat mild than the critical stress distribution along the cracking direction. Another possible reason for the discrepancy can be the difference in radial crack patterns around the microVickers indents; while the radial cracks were well developed in previous studies [10, 11], the surface crack propagated imperfectly at low indentation load in this study. It means that the imperfect and partial cracking may be expected to have relatively small crack-opening displacement thereby producing lower peak cracking stress.

As discussed above, present nanocontact deformation method produced reasonable cracking stress levels and distribution behaviors comparing with previous studies

[5, 8, 10, 19–24] and it confirms that this technique can be a powerful tool applicable to various mechanical stress problems. Furthermore, this technique has various merits compared to previous contact stress measuring techniques. The distinctive features are summarized in Table 2 and compared with the previous indentation fracture mechanics test [8]; the nanocontact deformation method has superior spatial resolution and general applicability to ductile/brittle solids because it analyze stress influences from the nanocontact deformation itself. In addition, its nil directionality provides a testing simplicity but also puts a big obstacle in resolving biaxial stress components. The stress-elimination with microcracking attempted in this study can be a good solution of the stress resolution in brittle solids but in-depth researches including our pile-up study [25] must be followed for ductile metals.

Conclusions

Residual stress fields around microVickers indentation damages were directly characterized by using a stress-probing nanoindentation technique. The original damage stress in a biaxial state and its radial stress component remained after the subsequent microcracking brought about different shifts in the nanoindentation curve and these are converted to stress values by applying the stress-estimating model. The radial stress in the cracked corner showed a monotonic decaying of compressive stress against distance from the microVickers indent center while the average stress in the uncracked region showed a rise and fall behavior. The crack-opening circumferential stress, estimated by comparing the radial and average stresses, showed a rapid decaying behavior in positive sign and its peak value 406.7 MPa at the microVickers indent edge was comparable to the previous results of the critical cracking stress of soda-lime glass.

References

1. Lawn BR, Wilshaw TR (1975) J Mater Sci 10:1049
2. Lawn BR (1993) Fracture of brittle solids. Cambridge University Press, London, p 249
3. Lawn BR, Evans AG, Marshall DB (1980) J Am Ceram Soc 63:574
4. Anton RJ, Miskioglu I, Subhash G (1999) Exp Mech 39:227
5. Lucazeau G, Abello L (1997) J Mater Res 12:2262
6. Banini GK, Chaudhri MM, Smith T, Hayward IP (2001) J Phys D: Appl Phys. 34:L122
7. Zeng K, Rowcliffe DJ (1995) Acta Metall Mater 43:1935
8. Kese K, Rowcliffe DJ (2003) J Am Ceram Soc 86:811
9. Pharr GM (1998) Mater Sci Eng A 253:151
10. Fett T, Burghard Z, Zimmermann A, Aldinger F (2004) Adv Eng Mater 6:914
11. Burghard Z, Zimmermann A, Rödel J, Aldinger F, Lawn BR (2004) Acta Mater 52:293
12. Lee Y-H, Kwon D (2003) Scripta Mater 49:459
13. Lee Y-H, Kwon D (2004) Acta Mater 52:1555
14. Sawa T, Akiyama Y, Shimamoto A, Tanaka K (1999) J Mater Res 14:2228
15. Hagan JT (1980) J Mater Sci 15:1417
16. Lathabai S, Rödel J, Dabbs T, Lawn BR (1991) J Mater Sci 26:2157
17. Oliver WC, Pharr GM (1992) J Mater Res 7:1564
18. Swain MV, Hagan JT (1976) J Phys D: Appl Phys 9:2201
19. Hill R (1971) Mathematical theory of plasticity. Oxford University Press, Oxford, p 97
20. Schwarzer N, Hermann I, Chudoba T, Richter F (2001) Surf Coat Technol 146–147:371
21. Yoffe EH (1982) Philos Mag A 46:617
22. Lawn BR, Evans AG (1977) J Mater Sci 12:2195
23. Ishikawa H, Shinkai N (1982) J Am Ceram Soc 65:C-124
24. Jung Y-G, Pajares A, Banerjee A, Lawn BR (2004) Acta Mater 52:3459
25. Lee Y-H, Takashima K, Higo Y, Kwon D (2004) Scripta Mater 51:887